Investigating γ-ray decay of excited ^{12}C levels with a multifold coincidence analysis

G. Cardella,[1,*] F. Favela,[1,†] N. S. Martorana,[2,3] L. Acosta,[4] A. Camaiani,[5] E. De Filippo,[1] N. Gelli,[5] E. Geraci,[1,2] B. Gnoffo,[2,1,6] C. Guazzoni,[7] G. Immè,[1,2] D. J. Marín-Lámbarri,[4] G. Lanzalone,[3,8] I. Lombardo,[1] L. Lo Monaco,[2] C. Maiolino,[3] A. Nannini,[5] A. Pagano,[1] E. V. Pagano,[3] M. Papa,[1] S. Pirrone,[1] G. Politi,[1,2] E. Pollacco,[9] L. Quattrocchi,[10,1] F. Risitano,[10,1] F. Rizzo,[2,3] P. Russotto,[3] V. L. Sicari,[7] D. Santonocito,[3] A. Trifirò,[10,1] and M. Trimarchi[10,1]

[1]*Istituto Nazionale di Fisica Nucleare Sezione di Catania, Catania, Italy*
[2]*Dipartimento di Fisica e Astronomia "Ettore Majorana," Università degli Studi di Catania, Catania, Italy*
[3]*Istituto Nazionale di Fisica Nucleare-Laboratori Nazionali del Sud, Catania, Italy*
[4]*Instituto de Física, Universidad Nacional Autónoma de México, Mexico City, México*
[5]*Istituto Nazionale di Fisica Nucleare Sezione di Firenze and Dip. di Fisica Università di Firenze, Firenze, Italy*
[6]*Centro Siciliano di Fisica Nucleare e Struttura della Materia, Catania, Italy*
[7]*Dipartimento di Elettronica Informazione e Bioingegneria Politecnico Milano and Istituto Nazionale di Fisica Nucleare Sez. Milano, Milano, Italy*
[8]*Facoltà di Ingegneria e Architettura, Università Kore, Enna, Italy*
[9]*Commissariat Energie Atomique - Institute de Recherce Fundamental law in the Universe, Saclay, Gif sur Yvette, France*
[10]*Dipartimento di Scienze Matematiche e Informatiche scienze Fisiche e della Terra, Università di Messina, Messina, Italy*

(Received 12 November 2020; revised 11 October 2021; accepted 11 November 2021; published 16 December 2021; corrected 5 January 2022)

Background: The γ decay of ^{12}C levels above the particle emission threshold plays a crucial role in the production of ^{12}C in astrophysical environments. The Hoyle state is fundamental in the helium-burning phase of red giant stars, while the 9.64-MeV level can be involved in higher temperature explosive environments.
Purpose: The aim of this work was to explore the feasibility of measuring the γ-decay widths of the 9.64-MeV state. The experiments were performed at Laboratori Nazionali del Sud of INFN (INFN-LNS), in Catania, using α and proton beams impinging on a carbon target.
Methods: The method used consists in the detection of all charged products and γ rays emitted in the reaction, in order to strongly reduce the background.
Results: Few events of γ decay of the 9.64-MeV level were observed in the reaction $\alpha + {}^{12}$C. Also the decay yield of the Hoyle state was measured in both the measured reactions $\alpha + {}^{12}$C and $p+{}^{12}$C.
Conclusions: The γ decay of the 9.64-MeV level is, inside error bars, in reasonable agreement with the yield recently reported in literature by measuring the ^{12}C residue. The observed yield is larger than previously accepted lower limit. Also, the decay yield of the Hoyle state seems larger than the one reported in literature, even if the limited statistics do not allow a definite conclusion.

DOI: 10.1103/PhysRevC.104.064315

I. INTRODUCTION

The Hoyle state of the ^{12}C nucleus, at 7.65-MeV excitation energy (for a review on its properties, see Ref. [1]), plays a crucial role in the nucleosynthesis processes in stellar environments and in particular in the phase of helium burning [2]. This level is involved in the ^{12}C production through the 3-α reaction [3–5]. The rate of such a process is governed by the Hoyle state total width, Γ, and partial widths, for photon emission Γ_γ and Γ_{rad}, total electromagnetic decay width including also pair conversion. Recent works have stressed that such 3-α reaction proceeds through a sequential process, with formation of a ^{8}Be nucleus, at the ground state (g.s.), and a subsequent reaction with a third α particle [6,7]. However, new attempts are still ongoing in order to observe a contribution of a hypothetical Efimov state near to the Hoyle state [8–10]. Moreover, recent works were performed to understand if and how the Hoyle state total and partial widths are modified in high-density environments due to interactions with neutrons and protons [11,12]. In any case, the small radiative width Γ_{rad} still remains a crucial ingredient of the process at standard nuclear pressure. Indeed, ^{12}C is formed mainly through the γ-ray decay mode and then it can be further processed in stars to build other elements.

The Hoyle state is a 0^+ level and its decay to the g.s. is characterized by a two-step γ-ray emission through the 4.44-MeV level. A recommended value for the $\Gamma_{\text{rad}}/\Gamma$ branching ratio of $4.12 \pm 0.11 \times 10^{-4}$ was suggested in Ref. [13], including a weighted average of previous measurements reported in the literature. Most of these data were based on the direct measurement of the recoiling ^{12}C in scattering experiments, induced by proton or α beams, following the method proposed in Ref. [14]. In the weighted average reported in

*cardella@ct.infn.it
†Present address: Instituto de Ciencias Nucleares, Universidad Nacional Autónoma de México, Mexico city, México.

Ref. [13], only one direct measurement of two γ rays was used [15]. In recent years, several experiments have been proposed in order to verify and to improve such data sets [16–20]. Among them, also a high-resolution angular correlation study of the two emitted γ rays was performed with Gammasphere [21]. Recently, a new result shows an unexpectedly large relative $\Gamma_{\rm rad}/\Gamma$ of about 6.2×10^{-4} for the Hoyle state [22].

In explosive environments, for instance, supernova type II explosions where the temperature can reach the range of 10^9 K (T9), an involvement of higher excited energy ^{12}C levels is expected (see Refs. [23,24] for the rate calculations as a function of the temperature). This is the case of the 3^- level at 9.64 MeV, or the 2^+ level, belonging to the Hoyle state based rotational band, reported to be around 10 MeV in Ref. [25]. For the 9.64-MeV level, the direct γ decay to the g.s. is possible, through an $E3$ transition, and a rather small width for such process $\Gamma_{\gamma 0} = 0.31(4)$ meV was evaluated through electron scattering experiments [26,27]. However, also the decay toward the 4.44-MeV level, through an $E1$ transition, is possible. Based on the Weisskopf estimate, the probability of the latter decay mode should be larger than the former. Chamberlin *et al.* attempted to measure also such total radiative width, using the method of the direct detection of the recoiling ^{12}C [28]. Due to the difficulties in the subtraction of ^{13}C contaminants, only an upper limit of 14 meV for $\Gamma_{\rm rad}$ with $\Gamma_{\rm rad}/\Gamma < 4.1 \times 10^{-7}$ was extracted. A complex experiment was realized at the RCPN Osaka laboratory in Japan to improve this result, using the ^{12}C(p, p') reaction on a solid hydrogen target [29]. The recoiling ^{12}C were detected by the Grand Raiden spectrometer. The measured yield is much larger than the accepted upper limits, although, as reported in their conclusion, systematic and statistical uncertainties were considerably large. Tsumura *et al.*, on the basis of their results, tried also to reconsider the 3-α reaction rate at large temperatures ($T_9 > 2$) with respect to the Nacre compilation [23].

In the present work, we show the results obtained in two experiments performed by measuring γ rays and charged products coincidences using the CHIMERA multidetector, installed at INFN-LNS [30]. The 4π CHIMERA multidetector allows us to identify and to measure charged particles, using 1192 silicon-CsI(Tl) telescopes. Furthermore, CHIMERA permits us to detect and identify γ rays, with a good efficiency, using the CsI(Tl) crystals of the telescopes [31]. In the first experiment, we used a proton beam, delivered by the Tandem INFN-LNS, at 24-MeV incident energy, impinging on a 17-mg/cm^2 carbon target. A second experiment was performed by using a 64-MeV incident energy α beam, delivered by the Superconductive Cyclotron of INFN-LNS, on a 100-μg/cm^2 carbon target. The use of the latter thin target allowed detection of also the recoiling carbon and application of the method that we called complete redundant measurement (CRM). This method, described in detail in Sec. II, allowed us to decrease the background, imposing constraints derived by the conservation laws (energy and linear momentum) [32]. With this method, data were extracted on the Hoyle state decay; we were also able to measure some events of the γ decay of the 9.64-MeV level in a direct way. The fourfold coincidence, with adopted constraints, allows us to reduce the background measured with the twofold coincidence measurement performed in Refs. [28,29] at the cost of an obvious reduction of statistics.

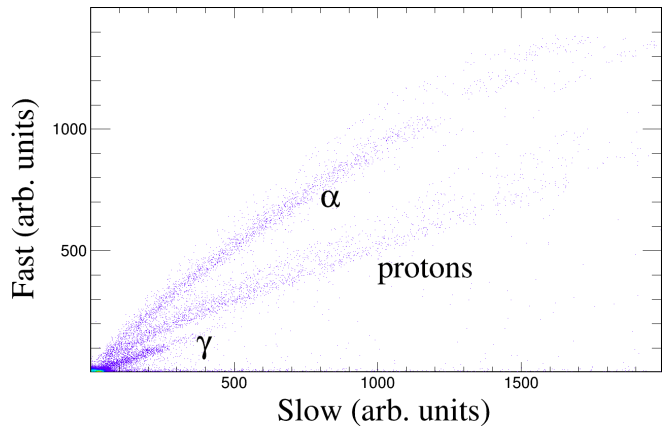

FIG. 1. Fast vs slow identification plot obtained in the reaction $\alpha + {}^{12}$C at 64 MeV with GET electronics [35].

Section II presents the experimental methods and shows the results obtained with the two experiments, underlining the effectiveness of the CRM method. The channel yield is discussed in detail in Sec. III, with a comparison among the different decay channels. In Sec. IV, conclusive remarks and perspectives are presented.

II. EXPERIMENTAL METHOD

The experiments were performed by using proton and α beams delivered by the accelerators of INFN-LNS in Catania. The proton beam, accelerated at 24 MeV, was delivered by the 15-MV Tandem while the α beam, accelerated at 64 MeV, was delivered by the Superconducting Cyclotron (CS). We used the 4π CHIMERA multidetector to detect charged particles and γ rays. CHIMERA is composed of 1192 Si-CsI(Tl) telescopes arranged in rings, covering 94% of the 4π solid angle. From 30° to 176°, 504 detection units are arranged in a spherical geometry, with the detector distanced 40 cm from the target. The opening angle of detectors belonging to this spherical part is $\Delta\theta = 8^\circ$ for the polar coordinate and $\Delta\phi = 11.25^\circ$ for the azimuthal coordinate. The 688 detection units are instead arranged in a cylindrical geometry, covering the forward region from 1° to 30°, to cope with the larger average particle yield. The CHIMERA multidetector was customized for charged particles and ions detection. However, CHIMERA can also be used to detect and to identify γ rays and neutrons; see, for instance, Refs. [31,33,34]. In detail, γ rays are identified using the pulse shape discrimination method (fast-slow technique) as shown in Ref. [33]. Figure 1 displays a pulse shape discrimination plot (fast vs slow components), showing the separation of particles and γ rays.

In order to decrease the elastic scattering contribution, only detectors belonging to the spherical region were included in the trigger. In the following, we will concentrate in the description of events detected in this spherical part. In the case of the experiment performed using the proton beam, standard

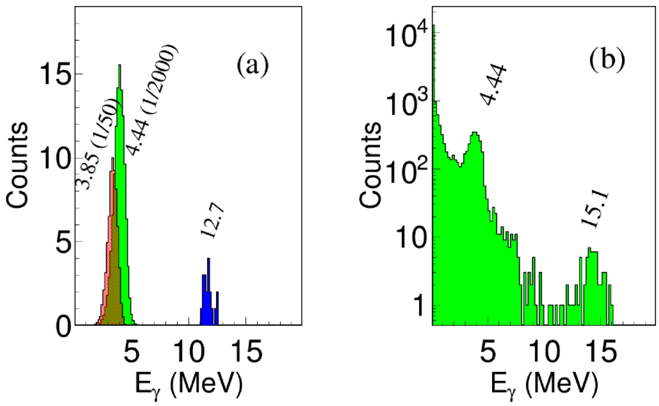

FIG. 2. (a) γ-ray energy spectrum for peaks at different energies, measured with the CsI(Tl) of the CHIMERA multidetector using the $\alpha + {}^{12}$C reaction. See text for details. (b) γ-ray energy spectrum, collected using a CsI(Tl) crystal with $p + {}^{12}$C reaction.

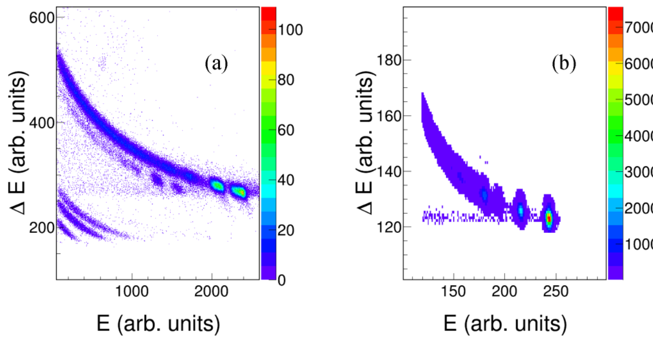

FIG. 3. (a) Identification plot $\Delta E - E$ measured for the reaction $\alpha + {}^{12}$C at 34°. The peaks relative to elastic, inelastic, and transfer channels can be observed. (b) Similar plot taken at 58° for the reaction $p + {}^{12}$C. Protons and few deuterons can be observed.

analog electronics was used. The experiment with the α beam was performed after upgrading the electronic front-end of the CsI(Tl) crystals, using a new digital electronics (GET) [35]. The full digitization of the signal wave forms allows us to extract more information on its shape, leading to better identification. Moreover, the new electronics measures also the arrival time of the particles in CsI(Tl), allowing us to better constrain the coincidence pattern. The energy resolution of CsI(Tl) detectors for γ rays at low energy (few MeV) is close to 10%, with a slight improvement at higher energy. Due to this resolution, we cannot discriminate the full energy and the escape peaks, for instance, at 4.44 MeV. Figure 2(a) shows an example of the energy response of γ rays at various energies. In this figure, one notes the peaks arising from the decay of the 4.44 MeV (green) and 12.7 MeV (blue) ^{12}C levels, and from the group of not resolved levels, from 3 to 3.8 MeV, of ^{13}C (red transparent). Such spectra were obtained using an α beam of 64 MeV and a carbon target, by selecting events in the opportune Q-value window and considering all the detectors. Figure 2(b) shows a similar spectrum, obtained for a CsI(Tl) crystal in the reaction $p + {}^{12}$C at 24 MeV. The $p + {}^{12}$C scattering allows to excite also the 15.1-MeV level. Using several peaks, we extracted the γ-ray energy calibration. The energy calibration takes into account that the response function of CsI(Tl) crystals is centered to the first escape peak γ-ray energy, as extracted by GEANT4 simulations [31].

The limited energy resolution observed in Figs. 2(a) and 2(b) is largely compensated, in the case of detection of isolated resonances, by the good detection efficiency guaranteed by the 4π coverage of the multidetector and by the large atomic weight of the scintillators. The evaluation of detection efficiency is discussed in Appendix A. Table I summarizes the results obtained for a single γ ray for the two experiments. One can note the large efficiency value evaluated for the 15.1-MeV level. However, this value is not very reliable due to the difficult evaluation of background for this peak and was not used in the evaluation of γ decay width. For the 12.7-MeV level, we extract a similar efficiency with both beams. This is due to the small influence for this level of energy thresholds. The larger thresholds of the old electronics, that was used with proton beam, are the main factor responsible for the 50% difference in the average efficiencies measured for the 4.44-MeV level.

Charged particles were detected and identified with the CHIMERA telescopes using the $\Delta E - E$ technique. Figure 3(a) shows an example of a $\Delta E - E$ plot of light particles, obtained using the silicon energy loss signal and the CsI(Tl) light signal, collected using the α beam. Proton, deuteron, triton, ^{3}He, and α particles are clearly visible. The ^{3}He and α lines show some populated regions. They correspond to the α particle elastic and inelastic scattering on ^{12}C and to one-neutron transfer reactions, populating ^{13}C ground and excited states. Figure 3(b) shows a similar plot, obtained using the proton beam. Only a few deuteron events and the proton line

TABLE I. Total efficiency evaluated for various levels using both proton and α beams. Data relative to 15.1-MeV level and obtained using the proton beam are taken at 58° (see Appendix A for details). The values reported in the fourth column are taken from Ref. [27].

Level	Reaction	Singles (counts/1000)	Yield 1γ [27] (%)	1γ (counts)	Measured 1γ eff. (%)
15.1	p + ^{12}C(58°)	24.5 ± 5	88	6496 ± 82	30 ± 6
15.1	p + ^{12}C(all)	–	88	11687 ± 109	–
12.7	p + ^{12}C	155.8 ± 10	1.93	628 ± 23	21 ± 2
4.44	p + ^{12}C	1042 ± 1	100	131793 ± 360	12.6 ± 0.2
12.7	α + ^{12}C	7 ± 1.4	1.93	28 ± 5	21 ± 6
4.44	α + ^{12}C	2491 ± 1	100	459205 ± 677	18.4 ± 0.2

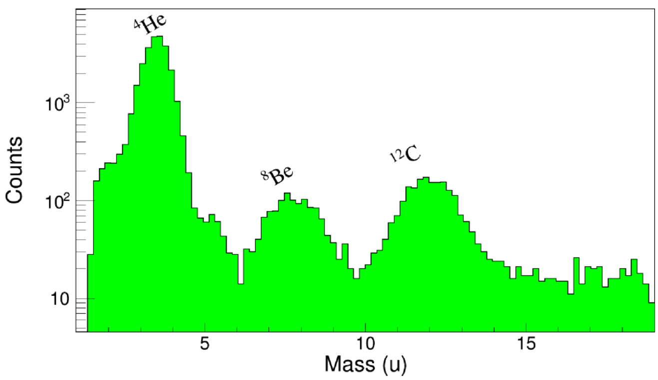

FIG. 4. Mass spectrum obtained through the measurement of the particle time of flight.

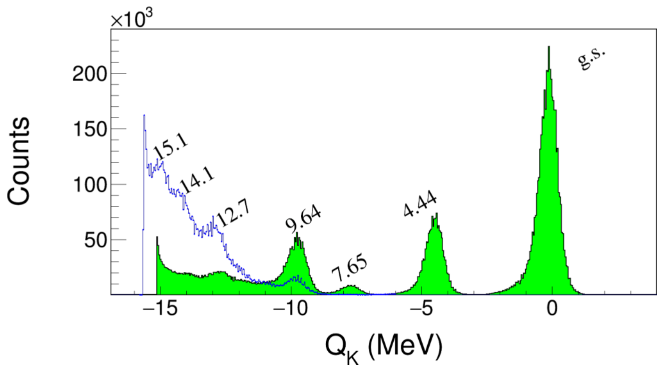

FIG. 5. Kinematic Q_K spectra in the reaction $p + {}^{12}C$ at 24 MeV for 66° (filled spectrum) and 58° (blue spectrum multiplied by 5). The observed excited levels are marked in the figure.

are observed. As aforementioned, in the α beam experiment, the carbon target thickness was 100 $\mu g/cm^2$ in order to make possible for the recoiling carbons and low-energy α particles (coming from the decay of excited carbon levels) to leave the target and to reach the detectors. Such particles, stopped in the first stage of the CHIMERA telescopes, were identified by using the time of flight (TOF) information. Figure 4 shows a mass spectrum obtained with this method. The TOF was measured sending to all TDC lines, as a common validated stop, the signal of the cyclotron radio frequency (RF), and, as a start, the time signal of the charged particle in the corresponding silicon detector. The detection angular range was limited at the spherical region of CHIMERA multidetector, where the distance between target and detector is only 40 cm. Being the time resolution of the beam packet of the order of 1 ns, a mass-by-mass identification cannot be achieved. However, scattered carbon ions can be perfectly discriminated from α particles and from ^{8}Be (two α particles in the same detector) that are the main products of the reaction. An accurate energy calibration was fundamental for the data analysis. Such a calibration was performed for both silicon and CsI(Tl) stages of the telescopes. This was obtained by using various calibration points and standard α sources. For silicon detectors, the energy loss of the various scattered projectiles (inelastically and elastically) on ^{12}C and Au targets was used (see Fig. 3). The pedestal position and the linearity were checked by using the calibrated pulsers of the apparatus. Moreover, in the case of the alpha beam, also the peak position of ^{12}C recoils was used, as evaluated by the kinematics, providing an additional calibration point for detectors at angles smaller than 90°. The used calibration points for particles stopped in the silicon detector (α source and recoiling carbon) and in transmission, ensured a good accuracy of calibration procedures. Second-order effects, as the target energy loss and the dead regions of the silicon detectors (0.5 μm silicon equivalent due to Al electrode and undepleted silicon layer), were also considered in the calibration procedure. The calibration of CsI(Tl) stage was performed by using the various elastic and inelastic proton peaks observed in the case of the proton beam, while for the case of the α beam, kinematical coincidences with scattered carbon ions were used to obtain narrower peaks for the α-particle calibration. This method was used in order to correct for the large energy spread produced by the opening angle of each detector.

A. The proton beam experiment

In the case of this experiment, we used a proton beam, accelerated at 24 MeV, and a carbon target of 17 mg/cm^2. The experiment was also used to perform γ-ray calibration of CsI(Tl) detectors in the study of the pygmy dipole resonance in ^{68}Ni [36]. Using the detected proton energy, it is possible to evaluate the kinematical Q-value spectra, following Eq. (1) based on energy and linear momentum conservation:

$$Q_K = (1 + m_3/m_4) \times E_3 - (1 - m_1/m_4)$$
$$\times E_1 - 2/m_4 \times \sqrt{(}m_1 \times m_3 \times E_3 \times E_1) \times \cos(\theta_3), \qquad (1)$$

where m_1 and E_1 are the mass and the energy of the beam; m_3, E_3, and θ_3 represent the mass, the energy, and the detection angle of the scattered projectile; and m_4 is the mass of the target-like scattered particle. Due to the small ratio of projectile and target mass, the variation with angle of the Q_K function is relatively small and, notwithstanding the $\Delta\theta = 8°$ opening angle of the detectors, we can well discriminate in the spectra the different levels populated in the reaction, as shown in Fig. 5. In such spectrum, we show the data collected at 66° (full green histogram) and at 58° (blue histogram multiplied by a factor of 5 for better visibility). At 58°, due to electronic thresholds, the g.s., 4, 44- and 7.65-MeV levels are not seen. The highest excited levels are instead better seen at 58° due to the smaller identification thresholds in $\Delta E - E$. Larger scattering angles were excluded in the analysis because the energy spread was too large in the thick target. We emphasize that in all spectra showed in this paper, the Q value was computed assigning to a particle the average angle of the detector. As shown in Ref. [37], this choice minimizes the experimental error. All the scattered proton events detected at 58° and 66° are plotted in log scale in Fig. 6 (filled green spectrum). At large negative Q_K values, one might observe sharp structures remnant because of the identification thresholds in different detectors. In the same figure, coincidence events with at least one γ-ray coincidence are plotted (red filled histogram). To produce this plot, we impose also a condition on the energy

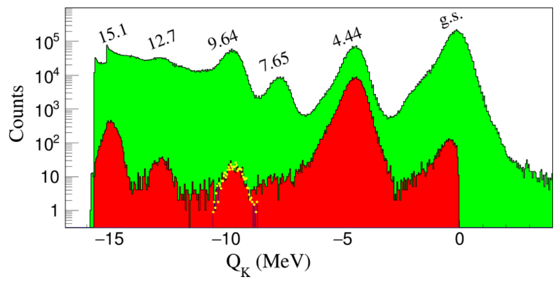

FIG. 6. Comparison of kinematic Q value measured in single (green filled spectrum) and one γ-ray coincidence events (red filled spectrum). A background spectrum evaluated for the 9.64-MeV level is also shown (dot yellow histogram).

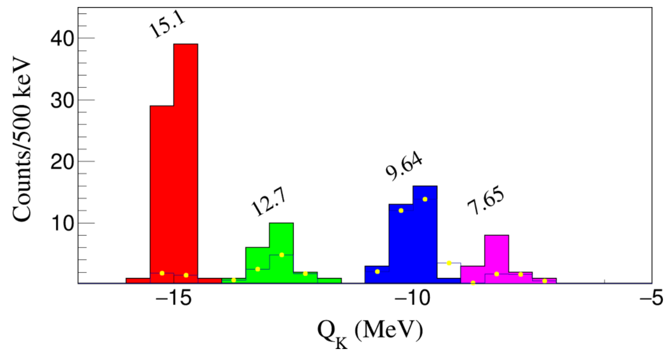

FIG. 7. Kinematic Q value evaluated for events in coincidence with two γ rays, with the expected total energy. Dot spectra are the background evaluated by looking at spurious coincidences with elastic peak.

conservation (Q_K must be equivalent to the γ-ray detected energy, within the experimental resolution). The γ-ray coincidence spectrum is dominated by the 4.44-MeV contribution. As better discussed in Appendix A, the efficiency reported in Table I was obtained by comparing these spectra. Both the 12.7- and 15.1-MeV levels that are embedded in the background in the single proton Q_K spectrum are clearly observed in the red filled histogram. The 15.1-MeV level is a $T = 1$ level that decays mainly by γ-ray emission (88%) [26,27]. The 12.7-MeV level is an unnatural (1^+) parity level having a large probability (nearly 2%) for γ-ray decay toward the g.s., and consequently, it can be very well seen to require one γ-ray coincidence. We note that the elastic peak is not completely suppressed and also a peak in the region of the 9.64-MeV level is present. Both these peaks are generated by spurious coincidences. This is quite obvious for the elastic peak and can be verified for the 9.64-MeV level. The amount of spurious coincidences can be evaluated by looking at random γ-ray coincidences with the elastic peak. These events can be normalized to the ratio between the single event yields of the 9.64-MeV and elastic peaks. The result is plotted as yellow dot histogram, for the 9.64-MeV level, in Fig. 6. We note that this background spectrum reproduces the observed rate of coincidence events for the 9.64-MeV level. The peaks at 15.1 and 12.7 MeV are genuine coincidences of yield much larger than the background, as will be better discussed in Sec. III.

Figure 7 shows the two γ rays' Q_K coincidence spectrum. In order to obtain this figure, we required the twofold γ-ray coincidence, imposing the condition on the total energy and requiring also a condition on the energy for each γ ray of the cascade. The same condition was applied in the background evaluation, for each analyzed levels. Again, spurious coincidences were evaluated by looking at random coincidences of γ rays with protons belonging to the elastic peak. Such background is shown as dotted spectra. As expected, the 15.1-MeV level is well above the background yield, a reasonable ratio of true to spurious coincidences is observed for the 12.7-MeV level, and for the 9.64-MeV level the peak to background ratio tends again to the value of 1. The Hoyle state has also a significative yield with respect to the background. From this experiment, we learn that in the case of Hoyle state a satisfactory background suppression can be obtained with triple coincidences measurement, imposing also the request of energy conservation. For the 9.64-MeV level, related to smaller decay widths, this background suppression method is not enough at least with our energy resolution. Therefore, in order to observe the decay of the 9.64-MeV level, we improved the background suppression, requiring also the measurement of a fourth coincidence particle, namely the recoiling nucleus. As will be better discussed in Sec. III, with around 3 million events belonging to the 9.64-MeV level we detected about 30 spurious coincidence events. In this way, we were able to perform in this region of energy a suppression factor of the order of 10^{-5} with two γ-ray coincidence.

B. The α beam experiment and the complete redundant measurement (CRM) method

The main idea under the CRM method is related to the observation that, in detecting all charged particles and γ rays emitted in a reaction, conservation laws can be used to clean the data from spurious coincidences and background events, and not only to extract Q-value information as in the case of the experiment with proton beam. Moreover, in our particular case, this implies a quadruple coincidence of two charged particles and two γ rays. The selection of coincidence time windows, allowed by the GET electronics adopted for CsI(Tl), strongly reduces the level of spurious coincidences. The α beam was chosen because of the larger momentum transferred to the recoiling carbon, allowing a simpler detection. Also, the α particles from the carbon decay have generally enough energy to be detected and identified with the ToF technique, as shown in Fig. 4. The disadvantage in the use of the α beam is to have a larger angular dependence of the Q_K value, as can be inferred by looking at Eq. (1). This generates in the detectors large peaks, as already observed in the identification plots of Fig. 3(a), and subsequently the Q-value spectra cannot be simply evaluated as in the case of the experiment with the proton beam. An example of the Q_K spectrum, obtained summing all detected particles, is shown in Fig. 8 (blue empty histogram). One notes that the separation between elastic and 4.44-MeV level is rather poor. The contribution of the Hoyle state cannot be observed being covered by the tails of the 9.64- and 4.44-MeV levels; therefore, Q_K cannot be used in this case. However, thanks to

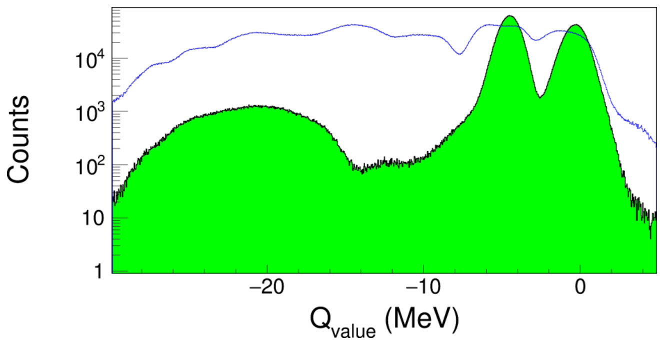

FIG. 8. Green filled spectrum is the Q_{ME}, obtained by evaluating the missing energy, as discussed in detail in the text. The blue spectrum is the Q_K, obtained considering the scattered α beam angle using Eq. (1). No conditions were imposed on this spectrum.

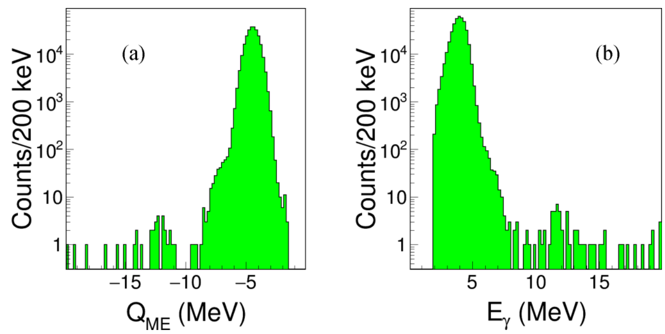

FIG. 9. (a) Missing energy Q-value spectrum measured in coincidence with one γ ray. The energy conservation is applied requiring γ-ray energy equal to the missing energy of charged particles. (b) γ-ray energy spectrum for the events of panel (a).

the complete event detection, we can measure the Q value using the energy conservation. We can then introduce a missing energy Q value (Q_{ME}), given by the difference between the total detected kinetic energy and the available beam energy. $Q_{ME} = \text{Energy}_{(\alpha \text{ scattered})} + \text{Energy}_{(^{12}\text{C})} - \text{Energy}_{(\alpha \text{ beam})}$. The Q_{ME} spectrum is plotted in Fig. 8 as full green histogram. To evaluate the Q_{ME} we need to detect and to identify also the ^{12}C in the correct time coincidence window. Moreover, a condition on the linear momentum conservation was also required to produce the plot. Q_{ME} is much better resolved than Q_K, partially recovering for the large kinematic spread seen by our detectors. The FWHM of the Q_{ME} peaks corresponding to the different levels are of the order of 1.5 MeV, mainly due to the energy resolution in CsI(Tl). The spectrum shows a slope change in the region of the Hoyle state and a bump at large negative Q values due to random coincidence events. We note a small enhancement in the region of the 12.7-MeV level. Even if the population cross section of this level is small, it can be seen, over the background, because of the relatively large ^{12}C production yield. Note that the $T = 1$ 15.1-MeV ^{12}C level, well populated with proton beam, is practically not populated by the interaction with α beam due to selection rules.

The background of the Q_{ME} spectrum is largely suppressed when the coincidence with at least one γ ray is required and the energy conservation is also applied. The elastic peak disappears and the 12.7-MeV level becomes more pronounced with practically no background, as shown in Fig. 9(a). The spectrum is dominated by the 4.44-MeV level as in Fig. 6. Figure 9(b) shows the corresponding γ-ray energy spectrum. Comparing the two spectra, it seems that the γ-ray spectrum is more resolved in energy. This is due to the smaller absolute error performed in the measurement of the relatively low γ-ray energy respect to the larger one, performed measuring the energy deposited by the α particle in the CsI(Tl) (30–40 MeV).

The constraint of a coincidence with a second γ ray allows us to observe the decay of the Hoyle state and other high excitation energy levels. The Q_{ME} and the γ-ray total energy spectrum observed with this constraint are shown in Figs. 10(a) and 10(b). There is still a small contribution of the tail of the 4.44-MeV level due to spurious coincidences, while most Compton-like events, in which the energy of the 4.44-MeV level was shared by two neighbor detectors, were subtracted with a cut on the minimum relative angle accepted between the two γ rays. The γ decay of the Hoyle state is well separated by the residual 4.44-MeV contribution. Despite the limited statistics of this experiment, some events are seen also in the 9.64-MeV region. Few counts were also observed near the region of the 12.7-MeV level.

C. Events kinematics

To better prove the reliability of the data we performed further checks. The most important one is to verify by reaction kinematic if the α particle and the recoiling ^{12}C follow the two-body kinematics. We used an extended Chamberlin method that includes also the γ-ray detection constraint adding energy conservation. Figure 11 shows a kinematic plot, in which the ^{12}C energy (y axis) is plotted as a function of the scattered α particle energy (x axis). Lines of different type and colors show the expected kinematic loci. In detail, in Fig. 11(a) all coincidence events between α particles and ^{12}C, as shown in Fig. 8 with the green histogram, are reported. Only the two kinematic loci of elastic and 4.44-MeV level are clearly populated; events of the 12.7-MeV level are also present, while other levels are overwhelmed by the background. Figure 11(b) shows the coincidence events with 2γ

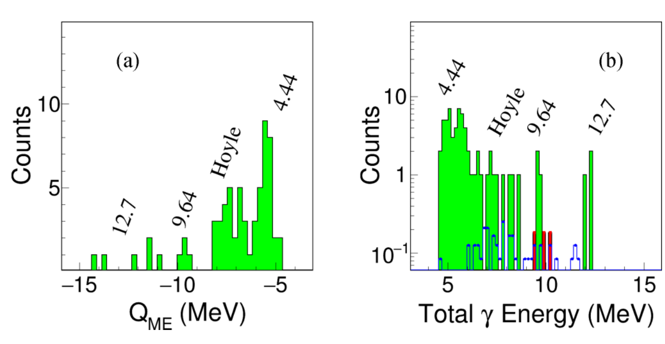

FIG. 10. (a) Q_{ME} and (b) total detected γ-ray energy in two γ-ray coincidence events (green filled spectrum). The red and blue histograms are background evaluations; see Appendix B.

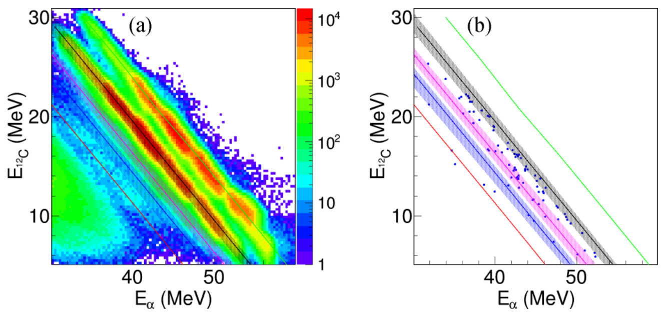

FIG. 11. Kinematic plot obtained with the energy of recoiling carbon plotted against the energy of scattered α particles. The green, black, purple, blue, and red lines correspond to the ground, 4.44-, 7.65-, 9.64-, and 12.7-MeV states; (b) events selected in coincidence with two γ rays.

rays and the required energy conservation. The contribution already observed in Fig. 10(a), arising from the tail of the 4.44-MeV level is still present, due to spurious coincidences. However, the line of the Hoyle state is well defined. The events observed for the 9.64-MeV level are closely located to the kinematic line, while the ones for the 12.7-MeV level are more spread.

D. Angular correlation analysis of detected γ rays

We performed also angular correlation analysis of the data, in order to exclude malfunctions and spurious effects that could simulate good events. More in detail, even if the number of γ-particle coincidences is quite small, we evaluated the relative angle distribution between the two detected γ rays, as recently reported in Ref. [21]. The number of detected events was scaled down by solid angle and efficiency (background was not subtracted). Figure 12(a) shows the results for the Hoyle state events. The distribution seems similar to the one measured in Ref. [21]. For the 9.64-MeV level, having only four events, the angular correlation is not significant. The important information in this case is that the events are spread over the whole detector, as observed also in Fig. 11(b) by looking at kinematic lines, and there are no particular clusters that could be produced by detector malfunctions.

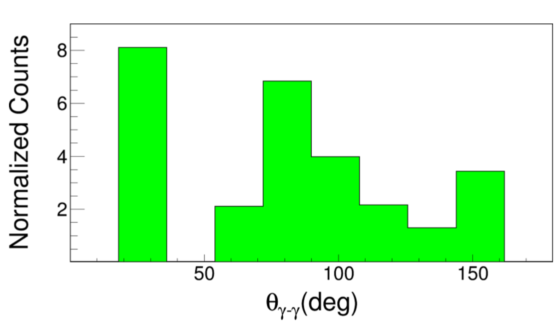

FIG. 12. Distribution of the relative angle between the two detected γ-rays from the Hoyle level. Counts were normalized to solid angle and detector efficiency evaluations.

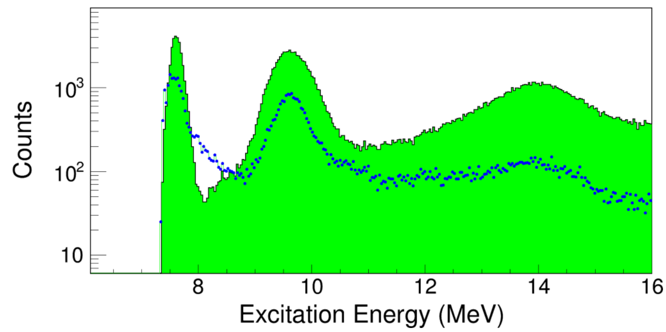

FIG. 13. Excitation energy calculated for events in which 3-α particles (filled green spectrum) or an α particle and a ^{8}Be events (blue dots) were detected in coincidence with the scattered beam α particle.

E. The 3-α decay channel analysis

In order to evaluate the 2γ-ray decay probability yield, it is necessary to measure also the production rate of the level. The Q_{ME} spectrum cannot be used to determine the total production yield over the particle emission threshold. As aforementioned, the kinematic Q_K is not useful in the experiment. However, the full angular coverage of CHIMERA allows us to detect, with relatively good efficiency, the most probable decay channel of Hoyle and 9.64-MeV levels, i.e., the 3-α channel. In this way, a direct comparison of the two decay channels is possible. Figure 13 shows the excitation energy spectrum of the 3-α events in coincidence with a scattered α particle (green filled spectrum). The excitation energy is obtained by summing the 3-α channel Q value with the center of mass energy of the 3-α particles. In the same figure, the blue dotted histogram shows the excitation energy spectrum evaluated by looking at ^{8}Be-α coincidences. As above reported, ^{8}Be corresponds to two α particles detected in the same detector and identified by using the TOF measurement (see Fig. 4). In Fig. 13, one notes that the 14.1-MeV level is less populated in the ^{8}Be-α spectrum with respect to the 3-α spectrum. Indeed, this level has a high probability to decay to

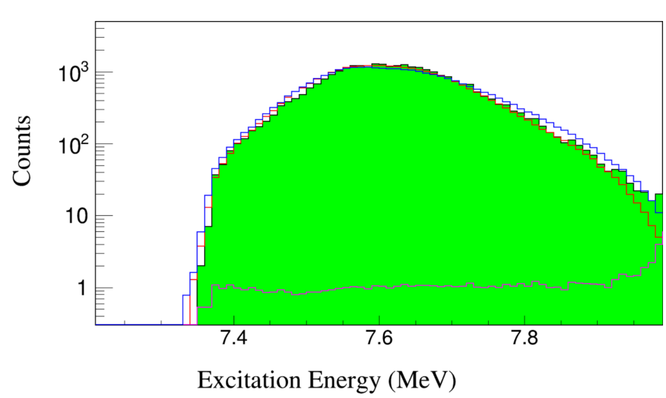

FIG. 14. Excitation energy spectrum of the Hoyle state (filled green spectrum) compared to simulations, red histogram with 2% of energy resolution and blue histogram with 5% of energy resolution. The ratio of experimental data and simulations with 2% of energy resolution is also plotted as purple histogram.

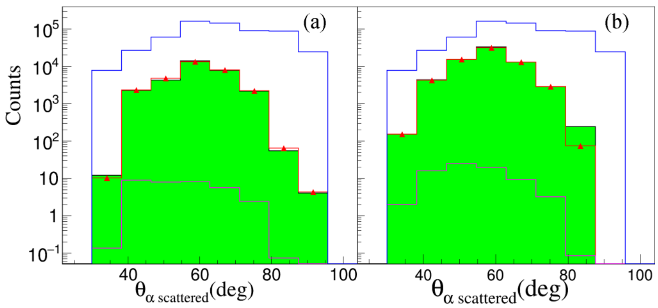

FIG. 15. (a) Observed angular distribution of scattered α particles populating the Hoyle state (filled green spectrum) compared to filtered simulations assuming 2% energy resolution shown as filled triangles and to not filtered angular distribution shown as blue histogram. The ratio of filtered over not filtered distributions is also plotted, multiplied by 100 as purple histogram showing the efficiency; (b) same as panel (a) but for the 9.64-MeV level.

the first excited state of ^{8}Be, so there is a lower probability to detect a ^{8}Be event in a single detector [38]. The detailed study of the decay mode of the observed levels is out of the task of this work and it will be presented in another paper in preparation.

The integral of the detected yield has to be corrected for the detection efficiency. This was evaluated by developing an event generator that simulates the sequential emission of the 3-α particles through the population of ^{8}Be g.s. following the reaction kinematics. Only α particles that pass the detector filter are included. The filter was based on the effective energy thresholds of detectors (around 2 MeV) and on the test of well-working calibrated detectors. The first step of simulation was to reconstruct precisely the measured excitation energy spectrum. The most important contribution to the width of the spectrum is connected to the angular resolution of our detectors. A smaller effect is due to the energy resolution that was evaluated around 2% (red histogram). A larger value such as 5% overestimates the high-energy side of the peak, as shown in Fig. 14 by the blue histogram. An important element of the simulation was also the reproduction of the angular distribution of scattered α particles. This can be obtained starting from the experimental one by some iterative procedure (the measured angular distribution must be corrected for the detection efficiency at different angles).

In Fig. 15, we plot the angular distributions of scattered α particles exciting the Hoyle state (a) and 9.64-MeV level (b) (filled histograms). The distributions are well reproduced by simulated data (red filled triangles) once the filter effect of the apparatus is activated. The distribution of simulated not filtered events, plotted as blue histogram, gives an idea of the efficiency variability as a function of the scattered α-particle angle also plotted in the purple histogram. We note a larger efficiency for the detection of Hoyle events due to the larger average laboratory energy of α particles allowing more easily to overcome energy thresholds. We evaluated from simulations the average detection efficiency of the different channels (3-α, α-^{8}Be). The probability to detect all α particles in different detectors is 79% for the Hoyle state and 87.5% for the 9.64-MeV level, first column of Table II. It is larger for this last level due to the larger CM energy available. The precision on evaluated efficiency is of the order of 5%. It was estimated by changing parameters as the energy resolution and input angular distribution. This precision can be also controlled by comparing the percentage of events 3-α detected for the two studied levels that can be extracted from data shown in Fig. 13. Correcting for the efficiencies the experimental events reported in Table II, we get the experimental value of 74% and 84% not far from expectations above reported. In total, we had about 200 kilo-counts (kcount) for the Hoyle state and 780 kcounts for the 9.64-MeV level. We underline that the detection efficiency for the Hoyle state and 9.64-MeV level were determined, neglecting the very small possibility of direct decay of the Hoyle state and assuming 100% decay through $^8\mathrm{Be}_{\mathrm{g.s.}}$ of the 9.64 MeV [6,7,38]. Both assumptions were well verified also by looking at experimental data. In Sec. III, the detection yields will be computed and discussed.

III. DECAY PROBABILITY DETERMINATION: RESULTS AND DISCUSSION

After the observation of the coincidence events, we must quantify such results extracting information on the decay probability. The yield evaluation is reported in Tables III and IV, for the experiment with the proton and α beam respectively and for the various levels observed in the reactions.

The single yields are reported in kilo-counts (kcount). The term *single* is used for events in which the γ-ray coincidence is not requested. These events correspond to proton counts in the case of $p + {}^{12}$C reaction. For the α beam, such events are evaluated as detailed in the previous paragraph and reported in Table II. The errors include also the background subtraction. In Subsecs. III A and III B, we will analyze the well-known levels at 15.1 and 12.7 MeV. We use them as a reference to check the correctness of the efficiency evaluations, assuming for their decay widths the values reported in literature [27]. This is done to demonstrate the ability of the detector to measure also low probability events as in the case of 2 γ-ray decay for the 12.7-MeV level. In Subsecs. III C and III D, we will discuss the Hoyle and 9.64-MeV level decay widths.

A. The 15.1-MeV level

From Ref. [27] (Table12.14), we know that the 15.1-MeV level has a width of 42 eV; its α-decay probability is only about 4%, while the γ-decay probability to the g.s. is about 88%. The remaining decay width is shared among various levels with a 2.2 ± 0.3% probability to decay to the 4.44-MeV level; in this case, a γ ray of 10.66 MeV is emitted. As previously mentioned, the 15.1-MeV level is excited only with the proton beam, being a $T = 1$ level. Its population yield is small and difficult to correctly evaluate, due to the large background, in the kinematic Q_k spectrum (see Figs. 5 and 6 green histogram). An attempt by using only data collected at 58° was performed in Table I but the large value of efficiency obtained is indicative of the scarce reliability of this value. In contrast, the one and two γ-ray coincidence spectra are almost background free (see Figs. 6 and 7). Therefore, in order to

TABLE II. Total efficiency evaluated with simulations for the 3-α events for the Hoyle and 9.64-MeV levels.

Level	Simul.		Effic. filtered		Detected		Tot. events
	3α (%)	$\alpha+{}^8$Be (%)	3α (%)	$\alpha+{}^8$Be (%)	3α ($\times10^3$)	$\alpha+{}^8$Be ($\times10^3$)	($\times10^3$)
7.65	79	21	19.2	25.3	28.5	13.0	199.8
9.64	87.5	12.5	10	14.2	65.5	17.5	778.2

verify the detection efficiency, the best option is to compare the one and two γ-decay yield with literature expected values. These decay probabilities can be expressed as follows:

$$\Gamma_{1\gamma}/\Gamma_{\text{tot}} = I_{1\gamma}/[I_{\text{single}} \times \epsilon(15.1)], \tag{2}$$

$$\Gamma_{2\gamma}/\Gamma_{\text{tot}} = I_{2\gamma}/[I_{\text{single}} \times \epsilon(10.66) \times \epsilon(4.44)], \tag{3}$$

where I (1γ, 2γ, and single) are the coincidence and single peak integrals, $\epsilon(x)$ is the detection efficiency of x MeV γ. Consequently, the decay probability through the 4.44-MeV level can be evaluated by using the ratio of $I_{2\gamma}/I_{1\gamma}$ as

$$\Gamma_{2\gamma}/\Gamma_{\text{tot}} = (I_{2\gamma}/I_{1\gamma}) \times [\epsilon(15.1)/\epsilon(10.66)] \times 0.88/\epsilon(4.44). \tag{4}$$

The efficiency ratio $\epsilon(15.1)/\epsilon(10.66)$ can be evaluated by GEANT4 (resulting in an average equal to 0.77), while for $\epsilon(4.44)$ we use the measured value reported in Table I. In Appendix A, it is shown that due to the 4π coverage of the apparatus errors due to γ-ray angular correlation are rather small and are included in the error bars. The final result, quoted in Table III, is that the decay through the 4.44-MeV level is around $3.1 \pm 0.6\%$ with respect to the total yield. This is in agreement, within error bars, with the $2.2 \pm 0.3\%$ value quoted in the literature [27]. Using the data on single counts taken at 58° we can evaluate also the 2γ-ray efficiency reported in Table III. As for the 1γ-ray efficiency, the obtained value seems too large due to the difficult evaluation of its background.

B. The 12.7-MeV level

The 12.7-MeV level is populated in both reactions. In the case of proton beam, we estimate its population by looking at the spectra of Fig. 5, obtained with protons detected at 58° and 66°. Having a larger cross section and being farther from identification thresholds with respect to the 15.1-MeV level, we can subtract the backgrounds and evaluate a yield around 156 kcounts. The efficiency reported in Table I was computed assuming for the γ-decay a probability of 1.93% [27]. As done before for the 15.1 MeV level, we evaluated the ratio of one- and twofold γ-ray coincidence by adapting expression (4). A value of $\Gamma_{2\gamma}/\Gamma = 0.23 \pm 0.12\%$ for the two γ-ray decay channel was obtained; this value is lower than the literature value of 0.29% reported in Ref. [27] but in agreement within the error bar. The same result is obtained by using expression (3) with the efficiency evaluated for the 8.27-MeV γ ray, by scaling the efficiency of the 12.7 level with GEANT4. We can calculate the same decay probabilities also in the α beam reaction. Due to the relatively large number of γ decays, 12.7 MeV is the only high energy level that can be observed in the Q_{ME} spectrum of Fig. 8 and in the kinematics plot of Fig. 11(a), despite the large background. The population of this level is so small that cannot be easily observed in the 3-α channel, and therefore we integrated the spectrum (in a range of ± 1 MeV) of Fig. 8 obtaining about 7000 counts, with background subtracted. With this value a reasonable efficiency of 21% (see Table I) was evaluated similar to the proton beam experiment and in agreement with GEANT4 calculations, taking into account the good working detectors. The case of 2γ decay due to the low population probability is less clear. For the proton beam, we had more than 150 kevents while here we have only 7000 events, so even if the efficiency for the detection of the 4.44-MeV γ ray is larger, the number of detected events is rather small and affected by some background. Even if there are three events in the total γ-ray energy spectrum of Fig. 10(b), only one seems really good in the Q_{ME} spectrum of Fig. 10(a), so the decay yield probability of about 0.28% with 100% error bar can be evaluated, as shown in Table IV.

TABLE III. Yield for two γ-ray coincidence events measured in the reaction $p+{}^{12}$C at 24-MeV incident energy. For the 15.1-MeV level, only the data collected at 58° are shown for which the single count value is available.

Level	Reaction	Singles (counts/1000)	Two γ (counts)	Effic. two γ (%)	Yield 2γ
15.1	$p+{}^{12}$C (58°)	24.5 ± 5	38 ± 6	5	–
15.1	$p+{}^{12}$C (all)		73 ± 9		3.1 ± 0.6 (%)
12.7	$p+{}^{12}$C	155.8 ± 10	12 ± 7	3.3	0.23 ± 0.12 (%)
9.64	$p+{}^{12}$C	2900 ± 11	-2 ± 8	–	–
7.65	$p+{}^{12}$C	278 ± 1	10 ± 4	1.6	$2.2 \pm 1.0\ 10^{-3}$

C. The Hoyle state and the 9.64-MeV level with proton beam

Having reasonably checked the efficiencies with the known levels, we can proceed to evaluate the decay width of the Hoyle state and of the 9.64-MeV level from the measured

TABLE IV. Evaluation of 2γ-ray yield measured in the reaction $\alpha+{}^{12}$C at 64 MeV. Singles are evaluated in Table II (total events) for the Hoyle and 9.64-MeV level, and for the 12.71-MeV they are reported from Table I.

Level	Singles (counts/1000)	Two γ (counts)	Effic. 2γ (%)	Yield 2γ
12.7	7 ± 1.4	1 ± 1	5.1	0.0028 ± 0.0028
9.64	778.2	2 ± 1.6	4.0	$6.4 \pm 5.1\ 10^{-5}$
7.65	199.8	12 ± 3.8	3.3	$1.8 \pm 0.6\ 10^{-3}$

coincidence events using Eq. (3) adapted to the different energies. We have collected about 280 kcounts in single and 10 events, background subtracted, in the 2γ-ray coincidence channel. We can evaluate in this way a decay probability of the state of about $2.2 \pm 1.0 \times 10^{-3}$ with a large error bar due to the background subtraction and efficiency evaluation. This decay yield is larger than the new result presented in Ref. [19] (6.1×10^{-4}). We note that the efficiency evaluated for the Hoyle state both in Tables III and IV is the smallest one due to the larger influence of detection thresholds on the 3-MeV γ-ray efficiency. The ^{13}C contribution can be neglected in this energy range, as evaluated with the α and proton scattering. Regarding the 9.64-MeV level, we are not able to draw any conclusive evaluation of the decay width, because the triple fold coincidence, at least with our energy resolutions, is not able to perform a good background suppression.

D. The Hoyle state and the 9.64-MeV level with α beam

In the α beam experiment, we observed 12 events (see Fig. 6) for the Hoyle state. Such events are confirmed by the kinematic plot of Fig. 11(b), while the maximum background was around one event (random plus ^{13}C backgrounds). The level population has to be evaluated from the 3-α decay channel, summing also the events detected as α + ^{8}Be, both shown in Fig. 13 and in Table II. Summing the two contributions, corrected for the efficiency, we can extract a yield for the Hoyle state production of about 200 kcounts. From this number, the decay probability is evaluated as $\Gamma_{2\gamma}/\Gamma = 1.8 \pm 0.6 \times 10^{-3}$, where the error takes into account also the efficiency evaluation. This value is consistent with the one measured in the case of proton beam but much larger than the result accepted in literature (4.1×10^{-4}) [5], and even larger than the most recently published value (6.1×10^{-4}) [19].

As anticipated in Sec. II, the observation of yield in the region of the 9.64-MeV level was quite unexpected. There are at least three counts in the total γ-ray energy and Q_{ME} spectra (Fig. 10) confirmed by kinematic plot of Fig. 11(b) (four events are very close to the kinematic line). The level of background from spurious coincidences and ^{13}C contamination is quite low, around 0.5 counts. The integral of the 3-α decay channel and ^{8}Be-α one are respectively about the values of 65 and 17.5 kcounts with small background. After the correction for the detection efficiency, we can evaluate a total population of the level of a little bit less than 800 kcounts. Considering two events, background subtracted, the relative decay yield value is $\Gamma_{2\gamma}/\Gamma = 6.4 \pm 5.1 \times 10^{-5}$. This direct measurement of the γ-ray decay cascade of this level is consistent with the recent result of Tsumura *et al.* [29] who reported $\Gamma_{\rm rad}/\Gamma_{\rm tot} = 1.3(+1.2-1.1)\times10^{-6}$. Despite the large error bar, the measured Γ_γ/Γ is more than one order of magnitude larger than the previously assumed upper limit value [28]. It is difficult to understand why results reported in the Chamberlin work [28] were so small. Looking in detail at their paper, one can speculate that the energy loss in silicon detectors' dead regions was not included in the evaluation of the threshold used to cut in the experiment α particles contamination from the rare carbon events.

Another important difference from our results and Chamberlin data is related to the ^{13}C background. This is due to the used method. In our experiment, we reduce strongly the ^{13}C background, requesting the 2γ-ray coincidences. Indeed, as reported by Chamberlin, a large background is given by the process in which the excited ^{13}C decays by emitting a neutron and an excited ^{12}C (4.44 MeV). In this process, we will have therefore events with only one γ ray in coincidence. By requiring two γ rays in coincidence and imposing a constraint on energy conservation, this background is reduced.

IV. CONCLUSIONS AND PERSPECTIVE

We have observed few events of the 2γ-ray decay channel of the 9.64-MeV level of ^{12}C. This was possible thanks to the ability of the CHIMERA multidetector to measure very small γ-ray decay branches by using the CRM method. The experiments performed have shown that the large efficiency of the multidetector and the simultaneous detection of particles and γ rays are very effective to reduce the background, which affects these measurements. The collected statistics prevent us from drawing definite conclusions from the obtained results; new measurements with increased statistics are needed. Also the γ-ray decay width measured for the Hoyle state is much larger than recent observations [22]. A possible explanation could be the presence of an Efimov state [8–10], near the Hoyle state, that we cannot discriminate in energy due to our energy resolution. If this state really exists and has, as expected [10], a large γ-ray decay width, our result could be influenced by such level.

The comparison of results collected using α and proton beams allows us also to understand the differences in the two ways of exciting the ^{12}C. Proton beam seems more efficient in the excitation of the 9.64-MeV level, at least at the beam energy and angles investigated. The importance of this level in the ^{12}C nucleosynthesis evidently grows by increasing the temperature of the source [23,29]; therefore the evaluation of an accurate decay width also for this decay branch is of crucial importance and new experiments should be planned to improve the statistical reliability of the result. In the future, we plan also to use the ability to detect both charged particles and γ rays with CHIMERA in order to investigate the γ-ray decay of excited light radioactive beams. Such beams will be produced after the high-intensity upgrade of the cyclotron ongoing at INFN-LNS and by the new FraISe (Fragment In-Flight Separator) facility under construction [39,40].

ACKNOWLEDGMENTS

We thank all INFN-LNS staff for the preparation and delivery of high-quality α and proton beams. This work was partially supported by the DGAPA-UNAM IN107820 grant and the "Programma ricerca di ateneo UNICT 2020-22 linea 2."

APPENDIX

In the following we discuss the evaluation of efficiency and the background evaluation.

APPENDIX A: EFFICIENCY EVALUATION

Detection efficiencies to γ rays (up to 60%) according to GEANT4 simulations are obtained for the scintillators of

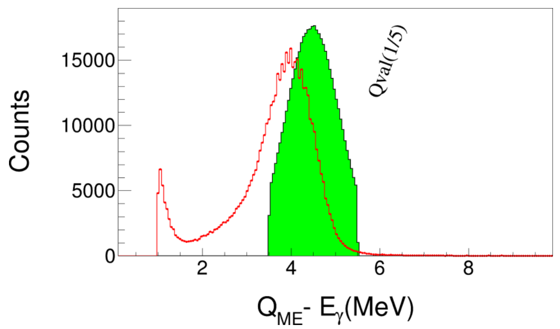

FIG. 16. Q value (filled green histogram) and corresponding γ-ray energy spectrum (red empty histogram) selected for the 4.44-MeV level in the $\alpha + {}^{12}$C reaction.

CHIMERA sphere, which have thicknesses ranging from 3 to 8 cm. The effective total efficiency, affected also by electronic thresholds and detector malfunctions, was measured using both proton and α beams, from the decay of ^{12}C levels (4.44, 12.7, 15.1 MeV). This total efficiency was measured by comparing the number of γ rays detected in coincidence with scattered particles, leaving the residual excited nuclei at the corresponding energy levels, and taking into account the expected γ-ray decay probability as evaluated in Refs. [26,27]. Figure 16 shows an example of this evaluation. In detail, the Q-value spectrum with selected events leaving the ^{12}C in the 4.44-MeV excited level is compared (scaled by a factor 5) to the γ-ray energy spectrum measured in coincidence with these particles in the whole CHIMERA multidetector (Q-value evaluation is explained in the main text). The comparison of the integrals of the two spectra (in the opportune energy window) gives the total detection efficiency reported in Table I. The efficiency variations, obtained with the proton beam with respect the α beam, are due to changes in the electronics and differences in detector malfunctions and thresholds. At low energy, the efficiency is more affected by electronic thresholds adopted for noisy channels. Checks were also performed in order to evaluate the angular correlation effects on the efficiency evaluation. The full angular coverage and symmetry of the detection system should minimize such effects on the global efficiency. As expected, by analyzing for instance the events relative to the 4.44-MeV level as a function of the ^{12}C detection angle we found a very small variation, of the order of 0.2%. This can be used as an error bar for the efficiency. The efficiencies not measured where estimated by GEANT4 calculations normalized to experimental measured data taking into account thresholds and not working detectors. The combined 2γ-ray efficiencies are reported in Tables III and IV.

APPENDIX B: BACKGROUND EVALUATION

In order to evaluate the background of the measurement, we performed various analyses on the data. There are at least two possible sources of background. The first one is due to spurious coincidences. For the proton beam, as described in the text, this background was evaluated using as reference the elastic peak. For the experiment performed with the α beam, this background was evaluated simply by moving the time coincidence windows obtaining a background level not larger than one count in the energy region spanning from the Hoyle state to 9.64 MeV. The second source of background is the coherent background generated by target impurities, mainly the 1.07% of ^{13}C present in the target. In order to evaluate this contribution, we used two different approaches. First, a direct approach undertaken performing a measurement with a 95% enriched ^{13}C target was used. The Q_{ME} spectrum measured with this target is shown in Fig. 17 as red histogram, compared with the data taken using the ^{12}C target (filled green spectrum). The normalization of the background was performed by comparing the elastic peaks measured with the two targets, assuming a similar cross section in the two cases, and therefore normalizing the measured spectrum to the expected content of ^{13}C in the target. This contribution is shown with red histogram in Fig. 10. A small contribution is present in the region of the 9.64-MeV level. Second, in order to improve the statistics of the background measurement, we used also the data from the one neutron transfer reaction channel observed in the experiment (see the ^{3}He line on Fig. 3). By using transfer reactions, we expect to populate a different window of angular momenta with respect to inelastic scattering, and indeed excited levels seem more populated than in the α scattering case (blue spectrum of Fig. 17). Therefore, the use of these spectra for the background estimation relies on scaling the spectra to the inelastic channels before applying the same scale factor of the ^{13}C target measurement. The obtained background contribution is plotted as blue histogram in Fig. 10. The two evaluated backgrounds are quite low with respect to the main target data. The scaled background integral in the region of the Hoyle state is less than 1 count and around 0.5 counts in the region of the 9.64 level.

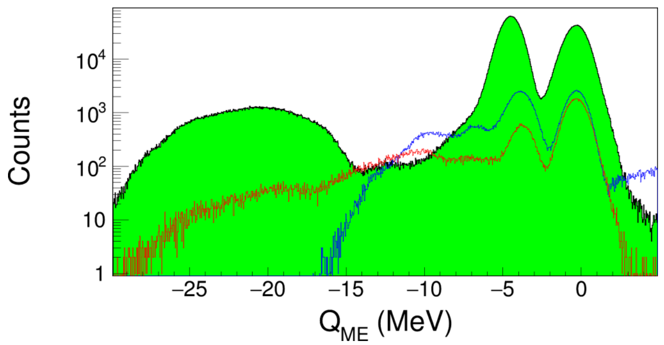

FIG. 17. Missing energy Q-value spectra for the reactions $\alpha + {}^{13}$C (red histogram) and $\alpha + {}^{12}\mathrm{C} \to {}^3\mathrm{He} + {}^{13}$C (blue histogram) compared to the spectrum $\alpha + {}^{12}\mathrm{C} \to {}^4\mathrm{He} + {}^{12}$C (green filled histogram), shown also in Fig. 8.

[1] M. Freer and H. Fynbo, Prog. Part. Nucl. Phys. **78**, 1 (2014).

[2] H. Schlattl, A. Heger, H. Oberhummer, T. Rauscher, and A. Csótó, Astrophys. Space Sci. **291**, 27 (2004).

[3] T. R. Bedding, B. Mosser, D. Huber, J. Montalbán, P. Beck, J. Christensen-Dalsgaard, Y. P. Elsworth, R. A. García, A. Miglio, D. Stello *et al.*, Nature (London) **471**, 608 (2011).
[4] F. Herwig, S. M. Austin, and J. C. Lattanzio, Phys. Rev. C **73**, 025802 (2006).
[5] F. Hoyle, Astrophys. J. Suppl. Ser. **1**, 121 (1954).
[6] D. DellAquila, I. Lombardo, G. Verde, M. Vigilante, L. Acosta, C. Agodi, F. Cappuzzello, D. Carbone, M. Cavallaro, S. Cherubini, A. Cvetinovic, G. DAgata, L. Francalanza, G. L. Guardo, M. Gulino, I. Indelicato, M. LaCognata, L. Lamia, A. Ordine, R. G. Pizzone, S. M. R. Puglia, G. G. Rapisarda, S. Romano, G. Santagati, R. Sparta, G. Spadaccini, C. Spitaleri, and A. Tumino, Phys. Rev. Lett. **119**, 132501 (2017).
[7] R. Smith, T. Kokalova, C. Wheldon, J. E. Bishop, M. Freer, N. Curtis, and D. J. Parker, Phys. Rev. Lett. **119**, 132502 (2017).
[8] H. Zheng, A. Bonasera, M. Huang, and S. Zhang, Phys. Lett. B **779**, 460 (2018).
[9] S. Zhang, A. Bonasera, M. Huang, H. Zheng, D. X. Wang, J. C. Wang, L. Lu, G. Zhang, Z. Kohley, Y. G. Ma, and S. J. Yennello, Phys. Rev. C **99**, 044605 (2019).
[10] J. Bishop, G. V. Rogachev, S. Ahn, E. Aboud, M. Barbui, A. Bosh, J. Hooker, C. Hunt, H. Jayatissa, E. Koshchiy, R. Malecek, S. T. Marley, M. Munch, E. C. Pollacco, C. D. Pruitt, B. T. Roeder, A. Saastamoinen, L. G. Sobotka, and S. Upadhyayula, Phys. Rev. C **103**, L051303 (2021).
[11] S. Jin, L. F. Roberts, S. M. Austin, and H. Schatz, Nature **588**, 57 (2020).
[12] M. Beard, S. M. Austin, and R. Cyburt, Phys. Rev. Lett. **119**, 112701 (2017).
[13] R. Markham, S. M. Austin, and M. Shahabuddin, Nucl. Phys. A **270**, 489 (1976).
[14] D. Chamberlin, D. Bodansky, W. W. Jacobs, and D. L. Oberg, Phys. Rev. C **9**, 69 (1974).
[15] A. W. Obst and W. J. Braithwaite, Phys. Rev. C **13**, 2033 (1976).
[16] M. Tsumura, T. Kawabata, T. Furuno, A. Koshikawa, M. Murata, T. Morimoto, S. Adachi, A. Tamii, K. Hatanaka, T. Ito *et al.*, J. Phys.: Conf. Ser. **863**, 012075 (2017).
[17] M. Tsumura, T. Kawabata, S. Adachi, T. Baba, T. Furuno, Y. Ishii, M. Murata, A. T. F. Kobayashi, Y. Kanada-Enýo, A. Tamii *et al.*, J. Phys.: Conf. Ser. **569**, 012051 (2014).
[18] W. Paulsen *et al.* (unpublished).
[19] T. Kibedi *et al.* (unpublished).
[20] T. Kawabata *et al.* (unpublished).
[21] M. Munch, M. Alcorta, H. O. U. Fynbo, M. Albers, S. Almaraz-Calderon, M. L. Avila, A. D. Ayangeakaa, B. B. Back, P. F. Bertone, P. F. F. Carnelli, M. P. Carpenter, C. J. Chiara, J. A. Clark, B. DiGiovine, J. P. Greene, J. L. Harker, C. R. Hoffman, N. J. Hubbard, C. L. Jiang, O. S. Kirsebom, T. Lauritsen, K. L. Laursen, S. T. Marley, C. Nair, O. Nusair, D. Santiago-Gonzalez, J. Sethi, D. Seweryniak, R. Talwar, C. Ugalde, and S. Zhu, Phys. Rev. C **93**, 065803 (2016).
[22] T. Kibedi, B. Alshahrani, A. E. Stuchbery, A. C. Larsen, A. Gorgen, S. Siem, M. Guttormsen, F. Giacoppo, A. I. Morales, E. Sahin, G. M. Tveten, F. L. Garrote, L. C. Campo, T. K. Eriksen, M. Klintefjord, S. Maharramova, H. T. Nyhus, T. G. Tornyi, T. Renstrom, and W. Paulsen, Phys. Rev. Lett. **125**, 182701 (2020).
[23] C. Angulo, M. Arnould, M. Rayet, P. Descouvemont, D. Baye, C. Leclercq-Willain, A. Coc, S. Barhoumi, P. Aguer, C. Rolfs *et al.*, Nucl. Phys. A **656**, 3 (1999).
[24] H. O. U. Fynbo, C. A. Diget, U. C. Bergmann, M. J. G. Borge, J. Cederkäll, P. Dendooven, L. M. Fraile, S. Franchoo, V. N. Fedosseev, B. R. Fulton *et al.*, Nature (London) **433**, 136 (2005).
[25] W. R. Zimmerman, M. W. Ahmed, B. Bromberger, S. C. Stave, A. Breskin, V. Dangendorf, T. Delbar, M. Gai, S. S. Henshaw, J. M. Mueller, C. Sun, K. Tittelmeier, H. R. Weller, and Y. K. Wu, Phys. Rev. Lett. **110**, 152502 (2013).
[26] F. Ajzenberg-Selove and C. Busch, Nucl. Phys. A **336**, 1 (1980).
[27] C. J. H. Kelley and J. E. Purcell, Nucl. Phys. A **968**, 71 (2017).
[28] D. Chamberlin, D. Bodansky, W. W. Jacobs, and D. L. Oberg, Phys. Rev. C **10**, 909 (1974).
[29] M. Tsumura, T. Kawabata, Y. Takahashi, S. Adachi, H. Akimune, S. Ashikaga, T. Baba, Y. Fujikawa, H. Fujimura, H. Fujioka *et al.*, Phys. Lett. B **817**, 136283 (2021).
[30] A. Pagano, M. Alderighi, F. Amorini, A. Anzalone, L. Arena, L. Auditore, V. Baran, M. Bartolucci, I. Berceanu, J. Blicharska *et al.*, Nucl. Phys. A **734**, 504 (2004).
[31] G. Cardella, L. Acosta, F. Amorini, L. Auditore, I. Berceanu, A. Castoldi, D. Dell'Aquila, E. De Filippo, L. Francalanza, B. Gnoffo *et al.*, Nucl. Instr. and Meth. in Phys. Res. Sect. A **799**, 64 (2015).
[32] F. Favela, G. Cardella, N. Martorana, L. Auditore, L. Acosta, A. Camaiani, E. De Filippo, S. De Luca, N. Gelli, E. Geraci *et al.*, J. Phys.: Conf. Ser. **1668**, 012004 (2020).
[33] M. Alderighi, R. Bassini, A Anzalone, I. Berceanu, J. Blicharska, C. Boiano, B. Borderie, C. Calí, R. Bougault, M. Bruno *et al.*, Nucl. Instr. Methods Phys. Res. Sect. A **489**, 257 (2002).
[34] A. Pagano, L. Auditore, and P. Russotto, EPJ Web Conf. **88**, 01001 (2015).
[35] E. Pollacco, G. Grinyer, F. Abu-Nimeh, A. Arokiaraj, T. Ahn, S. Anvar, H. Baba, Y. Ayyad, M. Babo, P. Baron *et al.*, Nucl. Inst. Methods Phys. Res. Sect. A **887**, 81 (2018).
[36] N. S. Martorana, G. Cardella, E. G. Lanza, M. L. Acosta, L. Auditore, M. V. Andrés, F. Catara, S. Luca, D. Dell'Aquila, E. De Dilippo *et al.*, Phys. Lett. B **782**, 112 (2018).
[37] A. Raduta, B. Borderie, E. Geraci, N. Le Neindre, P. Napolitani, M. F. Rivet, R. Alba, F. Amorini, G. Cardella, M. Chatterjee *et al.*, Phys. Lett. B **705**, 65 (2011).
[38] M. Alcorta, M. J. G. Borge, M. Cubero, C. A. Diget, R. Dominguez-Reyes, L. M. Fraile, B. R. Fulton, H. O. U. Fynbo, D. Galaviz, S. Hyldegaard, H. Jeppesen, B. Jonson, O. S. Kirsebom, M. Madurga, A. Maira, A. Munoz-Martin, T. Nilsson, G. Nyman, D. Obradors, A. Perea, K. Riisager, O. Tengblad, and M. Turrion, Phys. Rev. C **86**, 064306 (2012).
[39] P. Russotto, L. Calabretta, G. Cardella, G. Cosentino, E. D. Filippo, B. Gnoffo, M. La Cognata, N. S. Martorana, E. V. Pagano, R. G. Pizzone *et al.*, J. Phys.: Conf. Ser. **1014**, 012016 (2018).
[40] N. S. Martorana, Il Nuovo Cimento C **44**, 1 (2021).

Correction: The institution name in Affiliation 4 contained an error and has been remedied.